JOURNAL OF SOLID STATE CHEMISTRY 86, 116–124 (1990)

Powder X-Ray Crystal Structure of VO_2(A)

YOSHIO OKA[1]

Department of Chemistry, College of Liberal Arts and Sciences, Kyoto University, Kyoto 606, Japan

TAKESHI YAO

Department of Industrial Chemistry, Faculty of Engineering, Kyoto University, Kyoto 606, Japan

AND NAOICHI YAMAMOTO

Department of Chemistry, College of Liberal Arts and Sciences, Kyoto University, Kyoto 606, Japan

Received October 16, 1989; in revised form February 8, 1990

VO_2(A), a metastable phase of vanadium dioxide, was synthesized by hydrothermal treatment of $VO(OH)_2$. The powder X-ray structure analysis of VO_2(A) has been performed by the use of EXAFS and the Rietveld method; possible structure models based on the EXAFS results were examined by the Rietveld analysis. VO_2(A) has a tetragonal symmetry with a space group $P4_2/nmc$; a = 8.4336(7) Å, c = 7.6782(7) Å, and Z = 16. The structure consists of a three-dimensional framework of VO_6 octahedra. Four units of two edge-sharing octahedra are linked to each other by sharing corners forming a 2 × 2 square block in the c-plane. The blocks are piled up along the c-axis by sharing edges of the octahedra resulting in zigzag chains of V ions running along the c-axis. Taking the revealed structure into consideration, a comparison with the structure of VO_2(B) is made and a tentative mechanism of the phase transition in VO_2(A) is proposed.

Introduction

VO_2(A), as well as VO_2(B), is one of metastable vanadium dioxides with respect to the stable phase of the rutile-type VO_2. The formation of VO_2(A) was first reported by Théobald *et al.* (*1*) in their extensive studies on hydrothermal reaction of the VO_2–$VO_{2.5}$–H_2O system; VO_2(A) was precipitated at reaction temperatures between 220 and 330°C from a suspension of V_2O_3 and V_2O_5 with an average oxidation number of V being 4.0, in which VO_2(B) and the rutile-type VO_2 were also obtained below 220°C and above 320°C, respectively. To our knowledge, VO_2(A) has not yet been obtained by any method other than hydrothermal treatment. They showed that VO_2(A) had a tetragonal symmetry (a = 11.90 and c = 7.68 Å), but the crystal struc-

[1] To whom correspondence should be addressed.

0022-4596/90 $3.00

ture remains unknown (*1*). In contrast to VO_2(A), VO_2(B) has also been obtained as an intermediate product in the course of the thermal reduction of V_2O_5 by H_2 or SO_2 gas (*2, 3*) and its structure has been determined by Théobald *et al.* (*2*) which is related to those of V_2O_5 and V_6O_{13}.

Recently Oka *et al.* (*4*) have revealed a phase transition in VO_2(A) at 162°C by DTA, magnetic susceptibility, electrical resistivity, and high-temperature X-ray measurements. The transition is clearly observable on heating and the high-temperature phase gradually changes to the low-temperature phase on cooling. The features of the transition are that the magnetic moment of V^{4+} ion almost disappears in the low-temperature phase and the *a*-axis expands while the *c*-axis contracts through the transition on heating. Moreover the lattice period along the *c*-axis becomes half in the high-temperature phase. This behavior of the transition bears a striking resemblance to that of the metal-insulator transition in the rutile-type VO_2 (*5–8*). However, the lack of the knowledge of the structure makes it difficult to elucidate the exact mechanism of the transition in VO_2(A) and therefore it is of interest to determine the crystal structure of VO_2(A).

In the present work, VO_2(A) was prepared by hydrothermal treatment of $VO(OH)_2$. The structure of VO_2(A) was analyzed on powder samples by the following procedure utilizing the EXAFS and the Rietveld method. On the basis of the V–V distances and coordination numbers obtained by the EXAFS study structure models were given, from which the correct one was determined and was refined by the Rietveld method. A new VO_2 structure consisting of a three-dimensional framework of VO_6 octahedra has been revealed. A comparison of the structure with that of another metastable VO_2(B) is made in terms of the arrangements of VO_6 octahedra. A mechanism of the above-mentioned phase transition is also speculated based on the crystal structure.

Experimental

VO_2(A) was prepared by a hydrothermal method using $VO(OH)_2$ as a starting material, which was a little different from that adopted in the previous study (*4*). Powder samples of $VO(OH)_2$ were obtained by treating a $VOSO_4$ aqueous solution added with NaOH at 150°C for 24 hr. In the next step, a suspension of $VO(OH)_2$ was treated at 250°C for 48 hr, in which $VO(OH)_2$ was changed into VO_2(A). The product was separated by filtration and was dried in vacuum.

The EXAFS experiments were carried out using a Rigaku RU-1000 X-ray generator with a Cu target (30 kV, 1000 mA) at High Intensity X-ray Laboratory of Kyoto University. The vanadium K-edge EXAFS spectra were taken in the transmission mode using a flat Ge(111) crystal monochrometer. The energy resolution was 10 eV in the vicinity of the Cu*K* edge. The data analysis was conducted according to the standard procedure (*9*): subtraction of preedge and postedge backgrounds, edge normalization, extraction of the EXAFS signal $\chi(k)$ (k: wave number of photoelectron) and Fourier transformation (FT) to give a radial structure function $\phi_3(r)$. Peaks arising from the V–V interaction in the $\phi_3(r)$ curve were extracted and were subjected to inverse Fourier transformation (IFT). The IFT curves were parameter-fitted based on the multishell models using ab initio calculated backscattering amplitude (*10*) and phase shift (*11*). The phase shift was corrected for VO_2(A) sample by using EXAFS data of the rutile-type VO_2 and its crystallographic information (*12, 13*).

X-ray powder diffraction data were collected by a Rad-B powder diffraction system of Rigaku corporation using a Mo$K\alpha$ radiation equipped with a curved-crystal

graphite monochrometer. The step-scanning technique was used: a step width 0.01°, a step time 15 sec, and a 2θ range 5 to 45.5°. Powder patterns were indexed by the aid of the computer programs for indexing X-ray powder patterns (*14*). The details of the Rietveld method employed in the present study were described elsewhere (*15*), thus a brief outline is given in the following. The calculated intensity at $2\theta_i$, $Y_{\text{calcd}}(2\theta_i)$, is expressed by

$$Y_{\text{calcd}}(2\theta_i) = \sum_{hkl} I_{\text{calcd}}(hkl) \cdot \Omega_{hkl}(2\theta_i) + Q(2\theta_i).$$

$I_{\text{calcd}}(hkl)$ is an integrated intensity of hkl reflection, which in the present case includes the orientation factor $\exp(-G\alpha_{hkl}^2)$, where G is an orientation parameter and α_{hkl} is an acute angle between $[hkl]$ and the direction normal to the oriented crystal plane. $\Omega_{hkl}(2\theta_i)$ is a Lorentz function to describe an individual profile. $Q(2\theta_i)$ is a quadratic function of $2\theta_i$ to give a background. The expressions of $I_{\text{calcd}}(hkl)$, $\Omega_{hkl}(2\theta_i)$, and $Q(2\theta_i)$ were given in Ref. (*14*). Structure refinements were performed so as to minimize the reliability index R_{wp} defined below,

$$R_{\text{wp}} = \left\{ \frac{\sum_i [Y_{\text{obsd}}(2\theta_i) - Y_{\text{calcd}}(2\theta_i)]^2}{\sum_i [Y_{\text{obsd}}(2\theta_i)]^2} \right\}^{1/2},$$

where $Y_{\text{obsd}}(2\theta_i)$ is the observed intensity at $2\theta_i$.

Results and Discussion

Structure Determination

Figure 1a shows a radial structure function of VO_2(A), where the peaks ranging from 2.10 to 2.80 Å (P_1) and from 2.80 to 3.45 Å (P_2) were assigned to the V–V interaction. The IFT curves of P_1 and P_2 are shown in Figs. 2b and 2c, respectively, together with the parameter-fit results which were obtained by assuming the overlaps of two V–V shells for P_1 and three V–V shells for P_2. The V–V distances obtained from P_1 are 2.878 Å with coordination number (cn) of 2 and 3.223 Å with cn of 3, and from P_2 3.491 Å with cn of 1, 3.826 Å with cn of 3, and 3.943 Å with cn of 1.

An X-ray powder diffraction pattern of VO_2(A) was indexed based on a tetragonal symmetry with a = 8.4336(7) Å and c = 7.6782(7) Å as listed in Table I. Powder samples were found to exhibit preferred orientation of crystal plane (110) and the effect of the orientation on the peak intensities are evaluated in Table I. There were 204 reflections in the 2θ range of the measurement. The $hk0$ reflections with $h + k$ = odd and the $0kl$ reflections with l = odd were found to disappear, which led to the possible space groups $P4_2/nmc$, $P4_2/ncm$, and $P4/ncc$. Guided by the EXAFS results and the space groups, possible structure models were constructed and their compatibility with the X-ray powder pattern was examined by the Rietveld method. As a result, the space group was found to be $P4_2/nmc$. Setting V atoms on the positions of 16*j* and O atoms on those of 16*j* (O(1)), 8*i* (O(2)), and 8*i* (O(3)), the structure refinements were performed leading to R_{wp} = 0.166. The calculated and observed X-ray profiles are presented in Fig. 2. The unit cell has 16 formular units of VO_2 (Z = 16) which gives the density of 4.035 g cm^{-3} being consistent with the observed value of 4.01 g cm^{-3}. The final atomic coordinates are listed in Table II. The V–V distances and coordination numbers are listed in Table III, which show no appreciable deviation from those of the EXAFS results especially for the V–V distances. There is a slight discrepancy in the coordination numbers because values of coordination number obtained by the EXAFS study are generally less reliable.

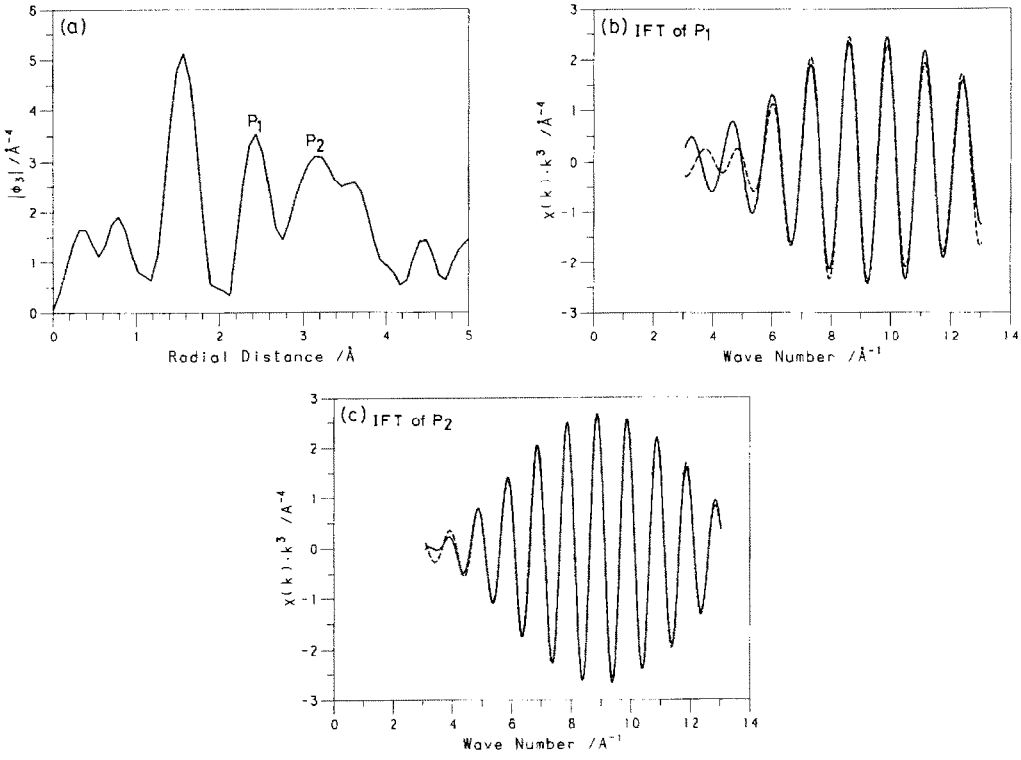

FIG. 1. EXAFS data for VO_2(A): (a) radial structure function; (b and c) inverse Fourier transforms (IFT) of the peaks P_1 and P_2 in (a), respectively. IFT ranges are 2.10 to 2.80 Å for P_1 and 2.80 to 3.45 Å for P_2. Solid and broken lines represent experimental data and parameter-fit results, respectively.

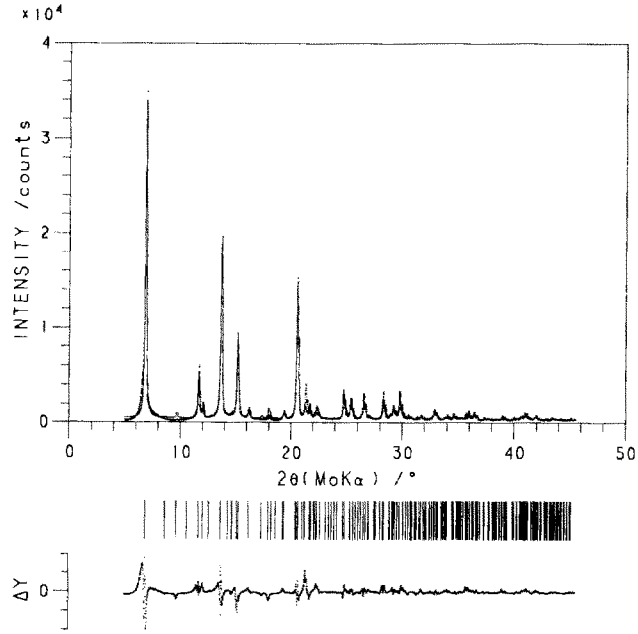

FIG. 2. Rietveld refinement plot of VO_2(A). The calculated and observed patterns are shown in the top by the solid line and the dots, respectively. The vertical marks in the middle show positions calculated for Bragg reflections. The trace in the bottom is a plot of the difference: observed minus calculated.

TABLE I

OBSERVED X-RAY POWDER DIFFRACTION PATTERN OF VO_2(A) FOR A Mo$K\alpha$ RADIATION

hkl	$2\theta_{obsd}$	$2\theta_{calcd}$	I/I_0[a]	I/I_0[b]
110	6.85	6.82	100	100
102	11.67	11.65	15	46
211	12.04	12.03	5	6
220	13.68	13.66	56	56
212	15.17	15.15	20	32
310	15.28	15.28	10	12
311	16.19	16.19	3	4
400	19.37	19.37	3	5
330	20.56	20.56	41	41
411	20.68	20.67	22	28
004	21.32	21.29	10	55
420	21.68	21.68	3	3
313	22.17	22.15	2	4
421	22.34	22.33	4	4
114	22.43	22.38	3	4
510	24.77	24.76	7	7
431	24.88	24.86	5	5
224	25.41	25.38	6	12
432	26.55	26.55	7	8
521	26.71	26.73	4	5
522	28.31	28.31	8	10
600	29.21	29.23	4	6
334	29.78	29.77	8	12
611	30.12	30.13	2	3
414	32.89	32.88	3	5
542	33.09	33.08	2	2
216	34.05	34.03	1	3
550	34.60	34.60	2	2
641	35.72	35.73	2	2
702	35.94	35.94	2	3
604	36.44	36.45	2	4
643	36.68	36.64	1	1
516	41.02	41.02	2	4
742, 812	41.14	41.15	2	3

Note. Tetragonal: a = 8.4336(7), c = 7.6782(7) Å.

[a] Observed intensity.

[b] Corrected for orientation effect.

TABLE II

POSITIONAL PARAMETERS FOR VO_2(A)

Atom	Position	x	y	z
V	16*j*	0.18936(3)	0.01764(4)	0.11787(10)
O(1)	16*j*	0.1674(1)	0.0012(2)	0.3743(3)
O(2)	8*i*	0.1634(1)		0.3416(3)
O(3)	8*i*	0.1352(1)		0.8930(5)

Description of the Structure

Figure 3 visualizes the structure of VO_2(A) projected on the c-plane. The structure basically consists of VO_6 octahedra. Four units of edge-shared two VO_6 octahedra are linked to each other by corner sharing forming a 2 × 2 square block in the c-plane. The square blocks, shifting to 1/2[110] and sharing edges of the octahedra, are superposed along the c-axis leading to a three-dimensional framework. The VO_6 octahedron and the stacking of the octahedra along the c-axis are depicted in Fig. 4. The VO_6 octahedron is slightly distorted as is seen from V–O distances and O–V–O angles listed in Table IV and the position of V ion is deviated from the center. The V–V distances along the c-axis are 2.8830 and 2.9019 Å which are shorter than that of 3.2078 Å in the c-plane and hence the V–V interaction should be stronger along the c-axis than in the c-plane indicating that zigzag chains of V ions are formed along the c-axis.

Comparison with the Structure of VO_2(B)

It should be of interest to compare the structure of VO_2(A) with that of VO_2(B) which is another metastable phase of VO_2. Both structures consist of three-dimen-

TABLE III

INTERATOMIC DISTANCES (Å) AND ANGLES (°) OF VO_6 OCTAHEDRON

V–O(1)^{i}	1.982(3)	V–O(1)^{ii}	1.885(3)
V–O(1)^{iii}	2.029(2)	V–O(1)^{iv}	2.227(2)
V–O(2)	1.993(2)	V–O(3)	1.784(2)
O(1)^{i}–V–O(1)^{iii}	86.6(7)	O(1)^{i}–V–O(1)^{iv}	81.8(8)
O(1)^{i}–V–O(2)	81.3(8)	O(1)^{i}–V–O(3)	99.4(9)
O(1)^{ii}–V–O(1)^{iii}	89.9(5)	O(1)^{ii}–V–O(1)^{iv}	84.6(5)
O(1)^{ii}–V–O(2)	99.2(7)	O(1)^{ii}–V–O(3)	94.4(9)
O(1)^{iii}–V–O(1)^{iv}	83.0(5)	O(1)^{iv}–V–O(2)	84.4(4)
O(2)–V–O(3)	85.2(4)	O(3)–V–O(1)^{iii}	107.7(8)

Note. The positions of oxygens are in reference to Fig. 4.

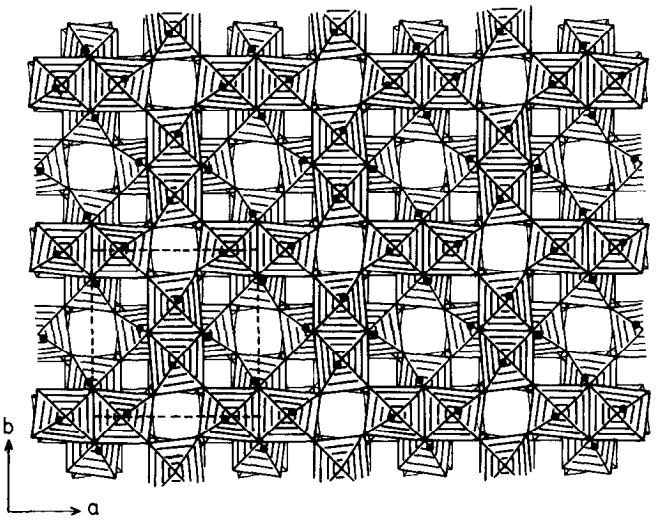

FIG. 3. Structure of VO_2(A) projected onto (001) plane. Closed circles are V ions and the unit cell is shown by the broken lines.

sional frameworks of VO_6 octahedra and VO_2(B) adopts a share structure derived from the structure of V_2O_5 in the same manner as V_6O_{13} (*2*). Figure 5 shows the arrangement of VO_6 octahedra (VO_6 sheet) in (110) of VO_2(A) (Fig. 5a) and (001) of VO_2(B) (Fig. 5b). It is seen that the VO_6 sheets in VO_2(A) and in VO_2(B) are isostructural, which are basically identical

TABLE IV

V–V DISTANCES (Å) AND COORDINATION NUMBERS (CN) FOR VO_2(A) OBTAINED FROM CRYSTAL STRUCTURE AND A COMPARISON WITH THE EXAFS RESULTS

Crystal structure		EXAFS data	
Distance	CN	Distance	CN
2.8830(17)	1	2.878	2
2.9019(18)	2		
3.1958(17)	1	3.223	3
3.2078(7)	1		
3.4945(9)	1	3.491	1
3.8506(16)	2	3.826	3
3.9153(13)	1	3.943	1

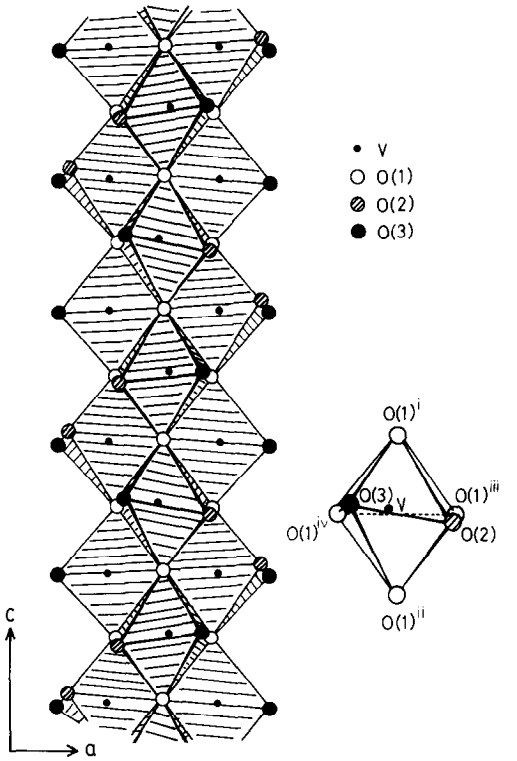

FIG. 4. VO_6 octahedron (right) and the arrangement of the octahedra linked along the *c*-axis (left).

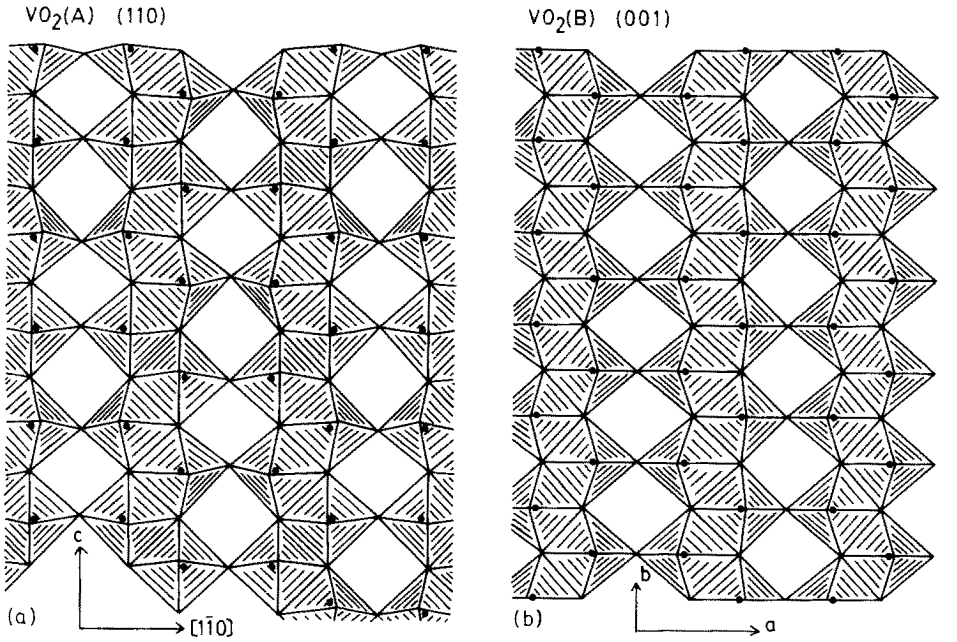

FIG. 5. Structures of crystal planes representing VO_6 sheets: (a) (110) of VO_2(A); (b) (001) of VO_2(B).

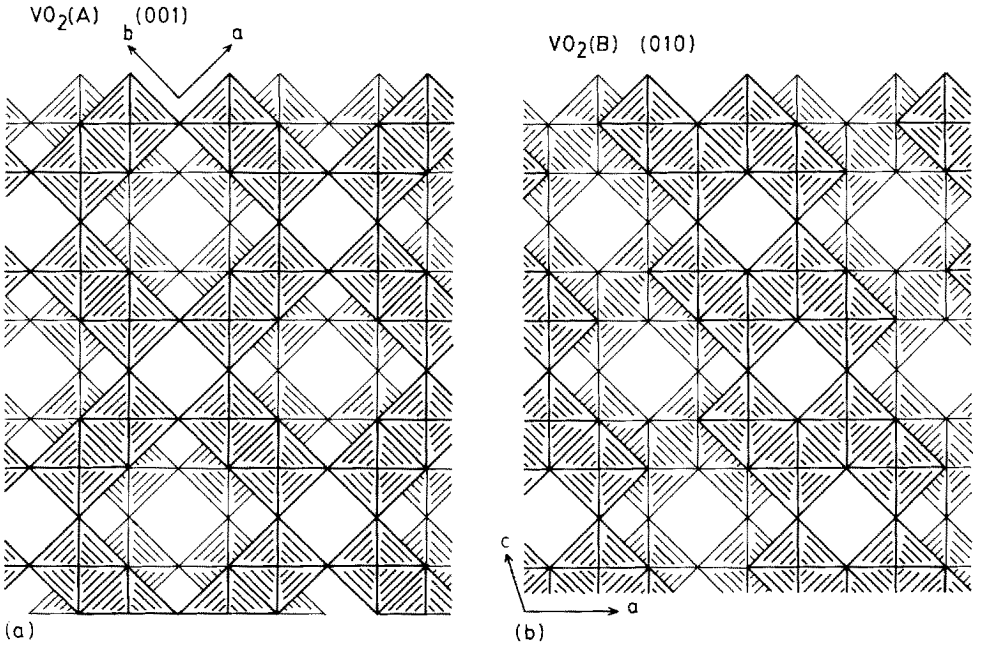

FIG. 6. Idealized structures showing superpositions of the VO_6 sheets: (a) VO_2(A) viewed along the *c*-axis; (b) VO_2(B) viewed along the *b*-axis.

with that in (001) of V_2O_5 (*16*). The difference of the structures between VO_2(A) and VO_2(B) is thus sought in the superposition of the VO_6 sheets. Figure 6 depicts idealized structures for (110) of VO_2(A) (Fig. 6a) and (010) of VO_2(B) (Fig. 6b) which represent the superposition of the VO_6 sheets. It is common to both structures that two VO_6 sheets form a layer unit which stacks in the direction of [110] in VO_2(A) and [010] in VO_2(B), but as is seen in Fig. 6 both the layer unit and the stacking mode are different between VO_2(A) and VO_2(B). In short, VO_2(A) and VO_2(B) consist of the VO_6 sheets of the same structures and the difference in the superpositions of the VO_6 sheets leads to the two distinct structures. Therefore, it is not by chance that VO_2(A) and VO_2(B) have nearly the same theoretical densities, 4.035 g cm^{-3} for VO_2(A) and 4.031 g cm^{-3} for VO_2(B). These values are considerably smaller than 4.657 g cm^{-3} for the rutile-type VO_2 implying that the two metastable VO_2 are less compact than the stable VO_2.

Possible Mechanism of the Phase Transition in VO_2(A)

As reported in the preceding paper (*4*), VO_2(A) exhibits a phase transition which appears to be similar to that of the rutile-type VO_2. In the rutile-type VO_2, V^{4+}–V^{4+} pairing along the *c*-axis of the rutile type is responsible for the phase transition from the high-temperature to the low-temperature phase (*17*). We suggested in the previous study (*4*) that such a V^{4+}–V^{4+} pairing was expected to occur in VO_2(A) along the *c*-axis, and it is considered based on the revealed structure that the pairing can be formed in the zigzag chains along the *c*-axis in the following manner. Figure 7 illustrates schematically the positions of V ions along the *c*-axis together with the projection on the *c*-plane. As shown in Fig. 7, V ions rotate cooperatively in the *c*-plane by about 5° around the *c*-axis with respect to the regular tetragonal positions which are located

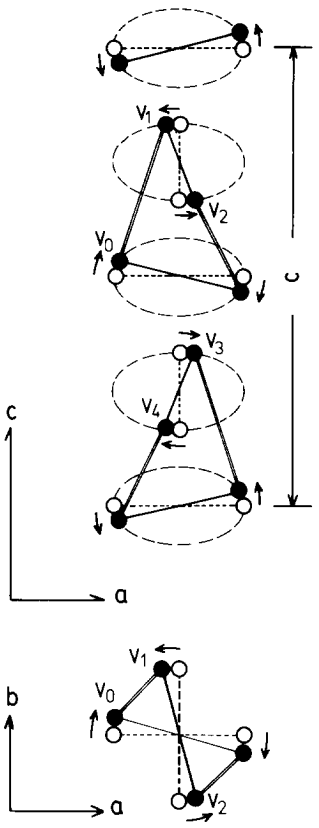

FIG. 7. Schematic representations of the mechanism of V^{4+}–V^{4+} pairing along the *c*-axis: side view (top); projected on the *c*-plane (bottom). Open and closed circles show V^{4+} ions in the regular tetrahedral positions and the actual positions, respectively. Arrows indicate the shift of V^{4+} ions from the tetrahedral positions and the resulting V^{4+}–V^{4+} pair is denoted by a double line. See text.

ideally in the center of the VO_6 octahedron. The directions of the rotation are denoted by arrows in Fig. 7 and consequently the V–V distances along the zigzag chains change to 2.883 Å (V_0–V_1 in Fig. 7) and 3.196 Å (V_0–V_2). The shorter V–V distance of 2.883 Å is denoted by the double line in Fig. 7. In this manner, V^{4+}–V^{4+} pairing is formed as a result of the cooperative rotation of V ions around the *c*-axis. However, other two V–V distances along the zigzag chain (V_0–V_3, V_0–V_4) become 2.902 Å which is not much larger than 2.883 Å. In

the high-temperature phase, V ions may occupy the regular tetragonal positions denoted by open circles in Fig. 7, which is consistent with the experimental fact that the lattice period along the *c*-axis becomes half (*4*). All the V–V distances along the zigzag chain are estimated to change to 2.961 Å at the transition. Further work is in progress to elucidate the exact mechanism of the phase transition with reference to that of the rutile-type VO_2.

Acknowledgments

The authors are grateful to Professors Koji Kosuge, Tsukio Ohtani, and Yutaka Ueda for valuable discussions. Thanks are also due to Professor Satohiro Yoshida for useful suggestions for the EXAFS experiments. The present work was partially supported by a Grand-in-Aid for Scientific Research from the Ministry of Education, Science and Culture.

References

1. F. THÉOBALD, *J. Less-Common Met.* **53,** 55 (1977).
2. F. THÉOBALD, R. CABALA, AND J. BERNARD, *J. Solid State Chem.* **17,** 431 (1976).
3. T. SATA, E. KODAMA, AND Y. ITO, *Kogyo Kagaku Zasshi* **71,** 647 (1968).
4. Y. OKA, T. OHTANI, N. YAMAMOTO, AND T. TAKADA, *Nippon Seramikkusu Gakujutsu Ronbunshi (J. Ceram. Soc. Japan.)* **97,** 1134 (1989).
5. F. J. MORIN, *Phys. Rev. Lett.* **3,** 34 (1959).
6. G. ANDERSON, *Acta Chem. Scand.* **8,** 1599 (1954).
7. S. WESTMAN, *Acta Chem. Scand.* **15,** 217 (1961).
8. S. MINOMURA AND H. NAGASAKI, *J. Phys. Soc. Japan.* **19,** 131 (1964).
9. B. K. TEO, "EXAFS: Basic Principles and Data Analysis," Springer-Verlag, Berlin (1986).
10. B. K. TEO, *J. Amer. Chem. Soc.* **101,** 2815 (1979).
11. A. G. MACKALE, B. W. VEAL, A. P. PAULIKAS, S. K. CHAN, AND G. S. KNAPP, *J. Amer. Chem. Soc.* **110,** 3763 (1988).
12. G. ANDERSON, *Acta Chem. Scand.* **10,** 623 (1956).
13. J. M. LONGO AND P. KIERKEGAARD, *Acta Chem. Scand.* **24,** 420 (1970).
14. T. YAO AND H. JINNO, *Nippon Kagaku Kaishi,* 529 (1980).
15. T. YAO AND H. JINNO, *Nippon Seramikkusu Gakujutsu Ronbunshi (J. Ceram. Soc. Japan.)* **96,** 1192 (1989).
16. H. G. BACHMANN, F. R. AHMED, AND W. H. BARNES, *Z. Kristallogr.* **115,** 110 (1961).
17. J. B. GOODENOUGH, *Phys. Rev.* **117,** 1442 (1960).